

# D4C glove-train: solving the RPM and Bongard-logo problem by distributing and Circumscribing concepts

Ruizhuo Song, Beiming Yuan

**Abstract**—This paper achieves significant progress in the field of abstract reasoning, particularly in addressing Raven’s Progressive Matrices (RPM) and Bongard-Logo problems. We propose the D2C approach, which redefines conceptual boundaries in these domains and bridges the gap between high-level concepts and their low-dimensional representations. Based on this, we further introduce the D3C method that handles Bongard-Logo problems and significantly improves reasoning accuracy by estimating the distribution of image representations and measuring their Sinkhorn distance. To enhance computational efficiency, we introduce the D3C-cos variant, which provides an efficient and accurate solution for RPM problems by constraining distribution distances. Additionally, we present Lico-Net, a network that combines D3C and D3C-cos to achieve state-of-the-art performance in both problem-solving and interpretability. Finally, we extend our approach to D4C, employing adversarial strategies to further refine conceptual boundaries and demonstrate notable improvements for both RPM and Bongard-Logo problems. Overall, our contributions offer a new perspective and practical solutions to the field of abstract reasoning.

**Index Terms**—Abstract reasoning, RPM problem, Bongard-logo problem.

## I. INTRODUCTION

DEEP neural networks have achieved remarkable success in various domains, including computer vision [1]–[3], natural language processing [4]–[6], generative models [7]–[9], visual question answering [10], [11], and abstract reasoning [12]–[14]. This success is primarily attributed to the remarkable capabilities of deep learning, which can recognize text, images, and sound data by learning the inherent patterns and representational hierarchies within sample data, thereby demonstrating analytical learning abilities similar to humans. Especially when addressing complex pattern recognition problems, the powerful capabilities of deep learning enable it to mimic human activities, further advancing the progress of artificial intelligence-related technologies. Its outstanding performance in speech and image recognition has surpassed previous technologies in terms of recognition accuracy.

This work was supported by the National Natural Science Foundation of China under Grants 62273036. Corresponding author: Ruizhuo Song, ruizhuosong@ustb.edu.cn

Ruizhuo Song and Beiming Yuan are with the Beijing Engineering Research Center of Industrial Spectrum Imaging, School of Automation and Electrical Engineering, University of Science and Technology Beijing, Beijing 100083, China (Ruizhuo Song email: ruizhuosong@ustb.edu.cn and Beiming Yuan email: d202310354@xs.ustb.edu.cn).

All authors contributed equally to this work.

However, despite these impressive accomplishments in deep learning, there are still a series of unresolved issues and challenges that require further research and exploration. For instance, research is ongoing on how to utilize the results of upperlayer training as initialization parameters for lowerlayer training, aiming to enhance the efficiency of deep model training. Additionally, layer-wise initialization training with unsupervised learning constitutes a significant strategy within the field of deep learning.

Especially in the domain of graphical abstract reasoning, the advancement of deep learning remains an active area of research. Although deep learning has achieved remarkable success in intelligent vision tasks, elevating machine intelligence to potentially higher levels, the academic community’s research on the abstract reasoning capabilities of deep learning has not ceased. Conversely, this has propelled the emergence of graphical reasoning problems. Graphical reasoning problems pose unique challenges for deep learning, including small and difficult-to-label datasets, the requirement for deep understanding of spatial relationships, shapes, and colors in graphics, demanding strong reasoning and innovation capabilities from models, necessitating a certain level of explanatory ability from models, and posing higher demands on models due to problem complexity and diversity.

To address these challenges, we need to further explore novel model architectures, training methodologies, and optimization strategies. This may encompass directions such as designing more effective deep learning models, refining model training methods, and enhancing dataset quality. Simultaneously, we also need to develop a deeper understanding of the essence and characteristics of graphical reasoning problems so that we can better leverage deep learning techniques to tackle these issues. In summary, while deep learning has made certain strides in graphical abstract reasoning, numerous problems still await our investigation and resolution.

The Ravens Progressive Matrices (RPM) [14] and Bongard problems [12], [13], for example, present learning requirements that span from perceptual processes to inferential capabilities.

### A. RAVEN and PGM

The RAVEN database [15], a distinctive collection of Ravens Progressive Matrices (RPM) problems [14], stands out for its particular design elements. Each RAVEN problem consists of sixteen images, with eight forming the essence of

the problem, termed as the stem, while the remaining eight constitute a pool of alternate choices. Subjects are tasked with selecting appropriate images from this pool, which, together with the stem images, form a 3x3 matrix of graphical patterns. The matrix is characterized by a progressive pattern of geometric images in the row direction, encompassing an underlying abstract concept. Figure 1 presents a concrete instantiation of a RAVEN case’s construction, shedding light on the methodology and general attributes of these problems.

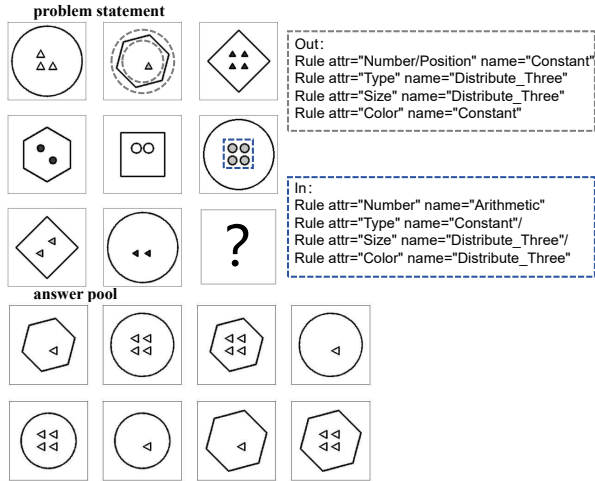


Fig. 1. RAVEN case

Within the design of RAVEN problems, geometric images often encompass human-predefined concepts such as "shape" and "color". However, these concepts are further abstracted in RAVEN problems into a finite, countable, and well-defined set of "visual attributes". The introduction of the term "rule" facilitates the description of how these "visual attributes" progress in a particular manner. It’s worth noting that not all visual attributes are constrained by this "rule"; some may be assigned randomly, posing additional challenges for deep model reasoning.

Constructing a comprehensive RAVEN problem entails initially randomly selecting a rule sample from a predefined rule set. Subsequently, corresponding visual attribute values are devised based on this chosen "rule". For attributes free from rules, their values are assigned randomly. Once these designs are in place, images are rendered according to the derived "attribute" information.

The RAVEN database not only encompasses problems with singular rules but also those with dual rules, elevating the level of difficulty and challenge. Specifically, the RAVEN database includes sub-databases with single rules such as center single, distribute four ( $G2 \times 2$ ), distribute nine ( $G3 \times 3$ ), among others. In problems with a singular rule, the progressive variation of entity attributes within the images is governed by one set of rules. Conversely, in problems involving dual rules, like in center single out center single (O-IC), up center single down center single (U-D), etc., the attribute progression must satisfy two independent rule sets.

The design approach of PGM [16] and RAVEN problems demonstrates a striking resemblance, with both frameworks

employing a problem format consisting of a stem composed of eight images and an answer pool formed by another eight images. It’s noteworthy that within the context of PGM problems, the concept of "rule" assumes a more profound significance. This concept not only delineates the progressive pattern of "visual attributes" along the row direction within the matrix but also imposes constraints on the progressive trend along the column direction. A representative instance of a PGM case is illustrated in the accompanying figure 2.

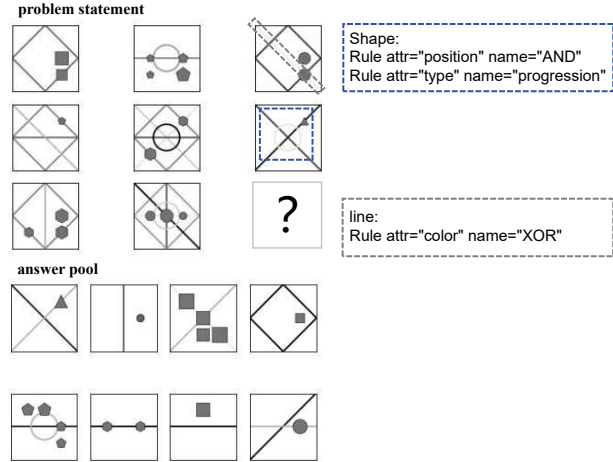


Fig. 2. PGM case

Given this complexity, the challenges associated with RPM problems extend beyond the mere exploration of visual attributes at various levels. They also encompass the crucial task of effectively inducing and learning the progressive patterns exhibited by these "visual attributes". Mastering and comprehending these progressive patterns hold profound implications for successfully tackling RPM problems, thereby underscoring their importance in this cognitive assessment domain.

### B. Bongrad-logo

The Bongard problem [12], [13] stands in stark contrast to the RPM problem, falling under the umbrella of small sample learning problems. Typically, Bongard problems consist of multiple images divided into two distinct groups: primary and secondary. Images within the primary group all convey an abstract concept that is bound by a specific rule, whereas images in the secondary group deviate from these rules in varying degrees. The crux of solving Bongard problems lies in the ability of deep learning algorithms to accurately classify ungrouped images into their respective categories. Notably, Bongard-logo [13] problems, a concrete instantiation of Bongard problems within the realm of abstract reasoning and a combination of a lot of Bongard-logo cases, pose a formidable challenge in terms of inferential complexity. Each Bongard-logo case comprises 14 images, including six images from both the primary and secondary groups, along with two images awaiting classification. The grouping criterion primarily relies on the geometric shapes present within the images and their arrangement. Figure 3 illustrates a representative Bongard-logo case, where every Bongard case consists of two sets of images:

Set A (primary) and Set B (auxiliary). Set A contains six images, with geometric entities in each image adhering to a particular set of rules, while Set B encompasses six images that do not conform to the rules observed in Set A. The task entails assessing whether the images in the test set align with the rules manifested in Set A. The level of difficulty varies depending on the case’s structural complexity.

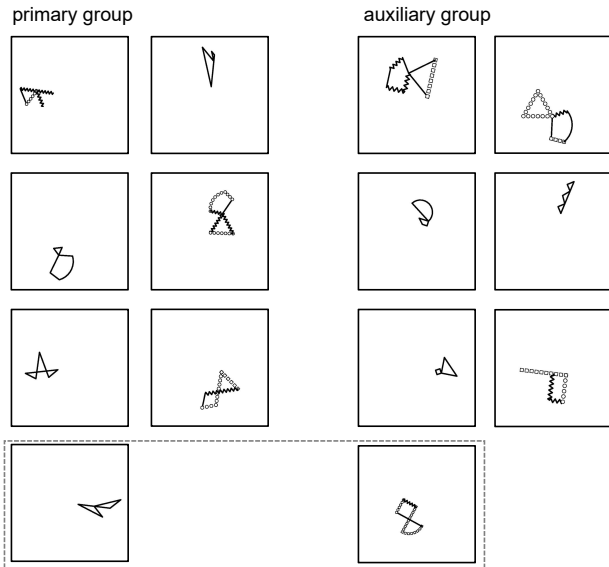


Fig. 3. Bongard-Logo case

Moreover, Bongard-logo problems can be further subclassified into three categories based on the concept domains they encompass: 1) Free-form problems (ff), where shapes are composed of randomly selected action strokes, with each image potentially housing one or two such shapes; 2) Basic shape problems (ba), which require recognition of a combination of one or two shape categories represented within the shape patterns; and 3) High-level concept problems (hd), designed to test a model’s ability to discover and reason about abstract concepts, such as convexity, symmetry, among others. Figure 1 exemplarily presents a specific Bongard-logo case alongside its underlying principles.

## II. RELATED WORK

### A. RPM solver

Discriminative models for image reasoning, such as CoPINet [19], LEN+teacher [18], and DCNet [20], offer diverse solutions with multi-dimensional outputs, focusing on learning differences, latent rules, and comparing disparities. NCD [22], SCL [23], SAVIR-T [24], and neural symbolism systems like PrAE, NVSA and ALANS [25]–[27] incorporate various techniques to improve reasoning accuracy and interpretability. By combining effective methods, RS-CNN and RS-TRAN [28] have achieved impressive results on the RPM problem. Triple-CFN implicitly extracts information on concepts and reasoning units, and “indexes” these reasoning unit information according to the concepts, achieving noteworthy reasoning accuracy. CRAB [29], based on a Bayesian

modeling approach, has established a highly customized “conservatory” that aligns seamlessly with its proprietary methodology, embodied in the creation of a new RAVEN database. This bespoke conservatory, despite forfeiting the inherent core challenges of RAVEN such as solution diversity and uncertainty, has facilitated remarkable breakthroughs for CRAB. Meanwhile, the scientific community eagerly anticipates the profound implications of this innovative approach for future research endeavors.

### B. Bongard solver

Researchers have tackled Bongard problems via three primary methods: language feature models, convolutional neural networks, and generated datasets. Depweg et al. used a formal language and symbolic vocabulary with Bayesian inference, but this struggled with complex problems and had scalability issues [12]. Kharagorgiev and Yun pre-trained on image datasets for feature extraction [30]. Nie et al. experimented with CNNs and meta-learning but had subpar results [13]. These methods have distinct strengths and weaknesses, underscoring the need for more research. Yuan introduced PMoC [31], a probabilistic model that measures the likelihood of auxiliary group samples fitting the main group’s distribution, a novel and effective approach. Notably, Triple-CFN [32] has successfully applied a uniform approach to both Bongard-Logo and RPM problems.

### C. Distribution distance measurement method

The formula for the Wasserstein distance [33] can be expressed as:

$$W(P, Q) = \inf \left( \sum ||X - Y|| \right) \quad (1)$$

where  $P$  and  $Q$  are two probability distributions, and  $X$  and  $Y$  are random variables sampled from  $P$  and  $Q$ , respectively. Here,  $||X - Y||$  represents the distance between  $X$  and  $Y$ , which can be the Euclidean distance, Manhattan distance, or other suitable metrics. The infimum (inf) denotes the minimum value among all possible mapping strategies. The Wasserstein distance is a measure of dissimilarity between distributions that accounts for the degree of difference between them, particularly suitable for handling non-uniform distributions and considering the shape and structure of the distributions. In the field of machine learning, the Wasserstein distance is widely used in generative models to evaluate the discrepancy between images generated by the generator and real images.

Sinkhorn distance [34] is a metric based on optimal transport, which approximates the Wasserstein distance through the introduction of entropy regularization, leading to increased computational efficiency. This distance satisfies the triangle inequality and is symmetric, but it is not a true distance metric since it converges to the Wasserstein distance only when the regularization term tends to zero. In each iteration, the Sinkhorn algorithm computes a new transportation plan based on the current one and updates the cost matrix, gradually reducing the cost of the transportation plan and approximating the optimal transport solution.

Under certain conditions, the Sinkhorn distance satisfies Lipschitz continuity. Specifically, if we consider two probability distributions with support sets in a compact metric space satisfying certain geometric conditions, the corresponding Sinkhorn distance can be shown to be Lipschitz continuous. This means that there exists a constant  $L$  such that for all probability distributions  $\mu'$  and  $\nu'$ , as well as  $\mu$  and  $\nu$ , the following holds:

$$S(\mu, \nu) \leq L \cdot d(\mu, \nu) + S(\mu', \nu') \quad (2)$$

where  $S$  is the Sinkhorn distance based on the cost function  $c$ , and  $d$  is an appropriate distance between these distributions (such as the Wasserstein distance).

The Lipschitz constant  $L$  typically depends on the choice of regularization parameters and cost functions. In practice, the Lipschitz constant may be difficult to compute directly but can be estimated through numerical experiments. It is worth noting that the Lipschitz constant often relates to the choice of cost function  $c$ . For instance, if  $c$  is a metric in the metric space (such as Euclidean distance), and the geometric properties of the space (like diameter or curvature) meet certain criteria, determining bounds for the Lipschitz constant becomes easier. However, for general cost functions and regularization parameters, determining the Lipschitz constant can be a highly complex task.

When the cost function for Sinkhorn distance is Euclidean distance, its Lipschitz constant depends on parameters of the Sinkhorn algorithm used and characteristics of the dataset, such as size, shape, and distribution. Additionally, Sinkhorn algorithm parameters, like the number of iterations and the weight of the regularization term, influence the continuity properties of the resulting Sinkhorn distance.

Therefore, to determine the Lipschitz constant for Sinkhorn distance with Euclidean distance as the cost function, specific dataset experiments and analyses are necessary to evaluate the continuity properties of the algorithm under different parameter settings. In applications involving Sinkhorn distance, particularly in machine learning and optimization problems, the focus is often on numerical stability and computational efficiency rather than strictly proving Lipschitz continuity or determining the Lipschitz constant. If strict theoretical guarantees are indeed required, detailed analyses of specific problem settings may be necessary.

#### D. Spectral normalization

Spectral normalization [35] is a stabilization technique for deep neural networks, particularly beneficial for generative adversarial networks (GANs). It controls the Lipschitz constant by normalizing weight matrices, ensuring outputs change proportionally to inputs. This regularizes the network, preventing overfitting and instability. In GANs, it stabilizes adversarial training, improving convergence and sample quality. Spectral normalization is computationally efficient and offers a direct way to control network complexity, making it a valuable tool for deep learning practitioners.

#### E. generative model

Wasserstein GAN [36] is a deep learning model that uses the Wasserstein distance as its loss function in Generative Adversarial Networks (GANs) to improve training stability and sample quality. By optimizing this distance, it effectively reduces mode collapse and enhances the realism and diversity of generated data.

DDPM (Denoising Diffusion Probabilistic Model) [9] is a generative model that models the transition from a real image to random Gaussian noise and vice versa to create new images. It involves a forward (diffusion) process adding noise and a reverse (denoising) process restoring the original image. The aim is to generate images ( $x'$ ) that are highly similar to real ones ( $x$ ), emphasizing realism and authenticity.

### III. METHODOLOGY

Both Bongard-logo and RPM problems [14] belong to the category of abstract reasoning problems, which require solvers to possess the ability to extract specific concepts from abstract entities. These specific concepts, compared to lower-level concepts such as “pixel arrangement and configuration styles”, possess a higher level of abstraction and incorporate prior knowledge from human perspectives to varying degrees, encompassing aspects such as shape, size, color, positional relationships, graph concavity and convexity, and graph closure. Bongard-logo and RPM problems employ different questioning approaches aimed at evaluating the solver’s proficiency in extracting and learning these abstract concepts.

This paper designs a new baseline model named Lico-Net for the RPM problem and achieves considerable performance on this problem. In addition, this paper extends the existing Bongard-Logo baseline in terms of model size and observes its limitations. Inspired by the limitations of the Bongard-Logo baseline, this paper designs the D2C method, which can be widely applied to RPM problems and Bongard-Logo, leading to improvements in model performance. This paper also designs the D3C method, which adheres to a core idea: representing complex, highly abstract human concepts with distributions rather than vectors is more appropriate. Finally, this paper designs the D4C method, which aims at the essence of abstract reasoning problems and contributes to RPM problems and Bongard-Logo problems.

### IV. DISCRIMINATOR OF CASE (DC)

In this section, to enhance our understanding and tackle the RPM (Raven’s Progressive Matrices) problem more effectively, we introduce a new baseline architecture, named Lico-Net. This innovative network is designed to address the unique challenges posed by RPM, leveraging advanced techniques and methodologies to achieve superior performance. Through a rigorous evaluation, we demonstrate the effectiveness of Lico-Net in solving RPM problems, paving the way for future research in this domain. Furthermore, we delve deeper into the previously established baseline network for the Bongard-Logo problem, critically examining its performance and limitations.

A. A novel baseline, Lico-Net, for RPM problem

The RPM problem requires participants to select answers from an option pool in order to complete a  $3 \times 3$  progressive matrix of images. If the completed matrix adheres to a specific image progressive pattern that can be inferred from the incomplete matrix (problem statement), it is considered a correct answer selection [39]. Therefore, a successful RPM discriminator is expected to be able to identify the rationality of the progression pattern within a complete  $3 \times 3$  progressive matrix.

We require an outstanding baseline, leading us to propose the Lico-Net (link-conception net) as a novel network for RPM solvers. Lico-Net is designed to assess the rationality of the image progression patterns within a complete  $3 \times 3$  RPM matrix, and to represent this rationality through a score. Accordingly, we can sequentially employ all the options provided in an RPM case to complete the problem matrix, leverage Lico-Net to evaluate the progressive rationality of the matrix, and assign scores to the options based on this rationality. This approach allows us to reason and solve RPM problems effectively. The design details of Lico-Net are described as follows.

Aligned with the current consensus among RPM solvers, which emphasizes the need for multi-scale or multi-viewpoint feature extraction from RPM images [23], [24], [28], Lico-Net incorporates the Vision Transformer (ViT) as a perceptron for feature extraction, while preserving the entire output vector, attention results, as multi-view point features. In this paper, we denote the number of viewpoints as  $L$ , a practice similar to that employed in Savirt [24], RS-Tran [28] and Triple-CFN. Lico-Net subsequently processes each viewpoint of extracted feature equally.

For the isometric viewpoint of an completed  $3 \times 3$  progressive matrix, we employ an MLP (Multi-layers perceptron) with a bottleneck structure to extract information from all minimal reasoning units (three images within a row for RAVEN and three images within a row or column for PGM) and obtain unit vectors. Specifically, we concatenate the representations of all images within a minimal reasoning unit in their inherent order and input them into the MLP. Compared to other structures, the MLP more directly preserves the order of the input representations and its structure is sufficiently simple. Due to the design of RPM problems, typically multiple minimal reasoning units must be combined to arrive at the image progression pattern of a RPM matrix. For instance, a RAVEN case requires at least two row unites to discern the case’s pattern, while PGM necessitates at least two row unites and two column unites [39]. It’s worth noting that determining the RPM matrix’s progression pattern doesn’t necessitate all minimal reasoning units; therefore, numerous combination methods of minimal reasoning units exist that are sufficient to identify the pattern. We refer to the combination requiring the least unit vectors as the minimal concept group.

Given that RPM problems might be constrained by multiple independent and decouple patterns, we embed  $N$  optimizable vectors within each minimal concept group (in this paper, we embed two optimizable vectors, with  $N$  being a hyperparameter that can be freely set) and input them

into a standard Transformer-Encoder as tokens to compute  $N$  progression pattern vectors for the progressive matrix in the case. Assuming there are  $M$  minimal concept groups, we have thus obtained  $N \times M$  progression pattern vectors under one viewpoint. We denote the progressive pattern vector from a single perspective as  $\{P_{nm} | n \in [1, N], m \in [1, M]\}$ . These vectors have additional purposes to fulfill. This paper independently calculates the scores of each option in the problem under  $N$  distinct pattern vectors.

The  $M$  minimal concept groups can be divided into two categories: those involving options and those not involving options. In this paper, we select the pattern vectors calculated from the concept groups not involving options as queries, and the pattern vectors involving options as keys and values. We then compute the multi-head cross-attention results between them and use a new MLP to score the attention outputs. Since we intentionally introduced  $N$  patterns, we obtain  $N$  scores, which are summed to yield the final score for one viewpoint. Finally, we calculate the overall score of one option by averaging the scores from all viewpoints. Aligned with the answer logic, we employ the Cross-Entropy loss function to constrain these scores for optimizing Lico-Net. It’s worth noting that we treat each dimension of the unit vector as a distribution and use covariance matrices as additional loss function term to control the correlation between these distributions, aiming to encourage the unit vectors to contain more information. The loss function  $\ell_{cov}$  attached to a batch of the minimal reasoning unit vectors  $\{U_{ij} | i \in [1, b], j \in [1, a]\}$  can be expressed as:

$$\begin{aligned}
 M_{cov}(\{u_{ij} | i \in [1, n], j \in [1, m]\}) & \\
 &= \frac{1}{n-1} \sum_{i=1}^n \sum_{j=1}^m (u_{ij} - \bar{u})(u_{ij} - \bar{u})^\top, \\
 \text{where } \bar{u} &= \frac{1}{n} \sum_{i=1}^n \sum_{j=1}^m u_i
 \end{aligned} \tag{3}$$

$$\begin{aligned}
 \ell_{cov}(\{U_{ij} | i \in [1, b], j \in [1, a]\}) & \\
 &= \frac{1}{d} \sum M_{cov}(\{U_{ij} | i \in [1, b], j \in [1, a]\})^2 \cdot (1 - I)
 \end{aligned} \tag{4}$$

Where  $b$  represents the batchsize for training the Lico-Net, and  $a$  denotes the count of minimal reasoning units within a single RPM case, which amounts to three in RAVEN and six in PGM.  $I$  represents the identify matrix. And  $d$  represents the dimension of unit vectors  $U_{ij}$ . The introduction of the covariance matrix as an additional loss function is an effective technique inherited from Triple-CFN, embodying its essence. The entire feedforward process can be depicted in figure 4.

In summary, after completing the RPM problem matrix with any given option, Lico-Net employs its perception module to encode each image within the problem matrix from multiple viewpoints, resulting in  $L$  sets of  $3 \times 3$  image representations. The subsequent reasoning module of Lico-Net processes these  $L$  sets of representations in parallel and equally. For any given set of representations, Lico-Net combines them to form all possible  $M$  minimal concept groups. Subsequently, Lico-Net extracts  $N$  progressive patterns from each minimal concept

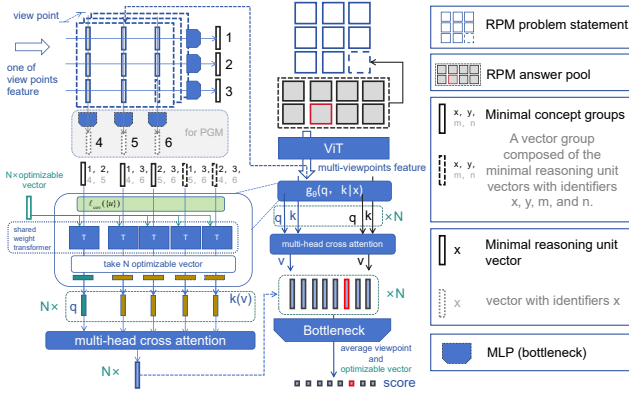


Fig. 4. Feedforward process of Lico-Net

group, totaling  $N \times M$  progressive patterns. Finally, Lico-Net utilizes an cross-attention mechanism to measure the consistency of each progressive pattern expressed by the  $M$  minimal concept groups and reflects this consistency through scores, resulting in  $N$  consistency scores. The final score for the option is determined by averaging these  $L \times N$  consistency scores.

### B. The baseline for Bongard-Logo problem

The cases designers of Bongard-logo drew from high-dimensional human concepts and knowledge, carefully categorizing the Bongard-logo database into three distinct problem types: FF, BA, and HD. This classification allows us to abstractly represent the distribution of the primary group in each Bongard-logo case as  $p_i(x|y)$ , while the distribution of the auxiliary group is denoted as  $q_i(x|y)$ . Here,  $y$  denotes the reasoning type of the case, which can take values from the set FF, BA, HD, and  $i$  represents the case index, ranging from 1 to  $n$ , where  $n$  is the total number of cases. Additionally, we denote the Bongard-Logo images as  $x_{ij}$ . Specifically,  $\{x_{ij}|j \in [1,6]\}$  represents images in the  $i$ -th primary group, while  $\{x_{ij}|j \in [8,13]\}$  represents images in the  $i$ -th auxiliary group. Additionally,  $x_{i7}$  represents the test image to be potentially assigned to the  $i$ -th primary group, and  $x_{i14}$  represents the test image to be potentially assigned to the  $i$ -th auxiliary group.

We copy a baseline from Triple-CFN, which refers to the baseline as  $f_\theta(z|x)$  that maps samples  $x_{ij}$  to latent variables  $z_{ij}$ . The baseline employs the InfoNCE loss function, which results in the  $f_\theta(z|x)$  being able to solve Bongard-logo to a certain degree. The InfoNCE loss function [41] can be mathematically expressed as:

$$\begin{aligned} \ell_{\text{InfoNCE}}(z_{pri}, \tilde{z}_{pri}, \{z_{aux_m}\}_{m=1}^M) \\ = -\log \frac{e^{(z_{pri} \cdot \tilde{z}_{pri})/t}}{e^{(z_{pri} \cdot \tilde{z}_{pri})/t} + \sum_{m=1}^M e^{(z_{pri} \cdot z_{aux_m})/t}} \end{aligned} \quad (5)$$

Where  $z_{pri}$  and  $\tilde{z}_{pri}$  represent distinct samples belonging to the primary group, and  $z_{aux_m}$  encompasses all  $m$  samples within the auxiliary group.  $m$  denotes the number of negative samples within a minimum learning unit, while  $t$  represents the temperature coefficient, and  $t$  is set  $10^{-3}$  in this paper.

Through the strategic employment of the InfoNCE function, we can circumvent the need to explicitly estimate the distributions  $p'_i(z|y)$  and  $q'_i(z|y)$ . Concurrently, this approach encourages enhanced similarity among the representations of the primary group encoded by the network  $f_\theta(z|x)$  and guarantees a greater degree of mutual exclusion between the representations of the primary and auxiliary groups. This process aligns with the underlying logic of Bongard-logo. InfoNCE can be construed as a loss function devised for the clustering of vector groups.

This paper reproduces the experiments for the baseline in Triple-CFN conducted based model ResNet50, which are individually implemented on the Bongard-logo database based on ResNet18. It focuses on the three concepts: 'FF', 'BA', and 'HD' for training, while concentrate on four test concept: 'FF', 'BA', 'NV' and 'CM'. Subsequently, a combined database was created by merging these three individual databases, and experiments were performed on this combined database. The experimental results are presented in Table I. The feedforward process is shown in figure 5.

The findings indicate that when presented with a combination of the three databases, the convolutional deep model experiences confusion among the three distinct human concepts. The varying degrees of reduction in the model's reasoning accuracy on the FF and BA problems, as well as the increase in accuracy on the generalization problems NV and CM, both clearly demonstrate this confusion. Furthermore, this confusion is not attributable to insufficient network capacity, as even the ResNet50 employed in this study, which is more capacious than the ResNet18 utilized in Triple-CFN's baseline, falls victim to the same predicament.

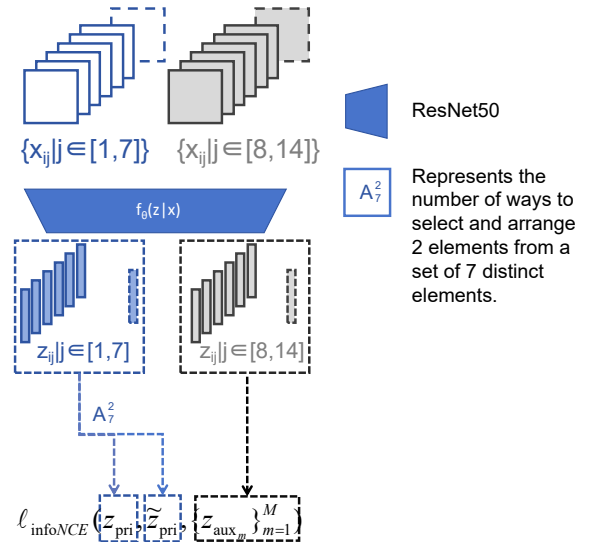


Fig. 5. Feedforward process baseline

This paper posits that, in the Bongard-Logo problem, the determination of image attributes relies heavily on the primary and auxiliary group samples within each case, which poses a fundamental challenge. It is precisely this multifaceted attribution of image properties that confuses deep networks when

TABLE I  
REASONING ACCURACIES OF DC BASED RESNET BASED RESNET50 ON BONGARD-LOGO.

Model and Data Set	Test Accuracy(%)			
	FF	BA	CM	NV
ResNet18 on Bongard-logo	88.1	97.9	76.0	75.8
ResNet18 on Separated Bongard-logo	97.9	99.0	75.0	72.8
ResNet50 on Bongard-logo	88.9	98.1	76.1	76.0
ResNet50 on Separated Bongard-logo	98.3	99.2	75.3	72.2

dealing with the three high-dimensional concepts inherent in the Bongard-Logo problem. Conversely, the RPM problem exhibits consistency in its recognition of image attributes. For instance, a white medium-sized triangle retains its attribute identification as such, regardless of its appearance in any RPM case option pool.

### V. DYNAMIC DELINEATION OF THE CONCEPT (D2C)

The determination of image attributes is significantly influenced by the specific contextual concepts associated with each individual case. Therefore, this paper aims to develop a method that effectively decouples the concepts across different cases. To accomplish this goal, we redefine the concepts within the Bongard-Logo database, representing them as conditional probability distributions  $p_i(x|Y_i)$  and  $q_i(x|Y_i)$ . Here,  $i$  ranges from 1 to  $n$ , representing each index of Bongard-Logo cases. Additionally, we introduce the notation  $\{Y_i^r | i \in [1, n]\}$  to denote the set of reorganized concepts. It can be seen that the number of reorganized concepts corresponds to the number of Bongard-Logo cases. Through this concept reorganization, we strive to achieve mutually exclusive expressions of concepts among all Bongard-Logo cases. In other words, each case is uniquely categorized based on its own distinct set of concepts, with corresponding unparalleled classification rules. By establishing a one-to-one relationship between image styles and these redefined concepts, we hope to enable the network to seamlessly infer concepts from the pixel arrangements of images.

In pursuit of fostering concept antagonism between differing problem domains, the present study has revised the data sampling techniques employed in mini-batch training methodologies. Furthermore, an additional loss function term has been designed to facilitate the reassignment of concepts within the network architecture. This method, denoted as ‘‘D2C’’(Dynamic Delineation of the Concept), strives to cultivate a state of concept contrast amidst diverse problem sets.

#### A. D2C phase 1: The concept delineation method based on a novel dynamic mini-batch sampling technique

Through a meticulous selection process, this paper identifies mutually exclusive pairs of Bongard-logo problems for training purposes and establishes concept antagonism within this triplet using the InfoNCE loss function.

Specifically, we encode a batch of Bongard-logo cases using ResNet50 and obtain a representation set  $\{Z_{ij} | i \in$

$[1, b], j \in [1, 14]\}$ , where  $i$  denotes the index of the Bongard-logo case within a batch, the batch size is  $b$ , and  $j$  represents the sample index within a single Bongard-logo case, with  $j \in [1, 7]$  being the primary samples and  $j \in [8, 14]$  being the auxiliary samples. From this batch of cases  $\{Z_{ij}\}$ , we deliberately choose two batches of cases  $\{Z_{tj} | j \in [1, 14]\}$  and  $\{Z_{\tilde{t}j} | j \in [1, 14]\}$ , ensuring that  $t, \tilde{t}$ , and  $i$  are all distinct. This process can be viewed as ancestral sampling. The extracted primary samples  $\{Z_{tj} | j \in [1, 7]\}$  and  $\{Z_{\tilde{t}j} | j \in [1, 7]\}$  are then incorporated into  $\{Z_{ij}\}$  as auxiliary samples, yielding an expanded set  $\{Z_{i\tilde{j}}\}$  where  $\tilde{j} \in [1, 28]$ . Subsequently, the InfoNCE loss function is computed for these newly formed sample groups  $\{Z_{i\tilde{j}} | i \in [1, b], \tilde{j} \in [1, 28]\}$ . The feedforward process, as illustrated in the accompanying diagram, involves a strategic misalignment of Bongard-logo problem batches to facilitate ancestral sampling during implementation. This process can be expressed as figure 6.

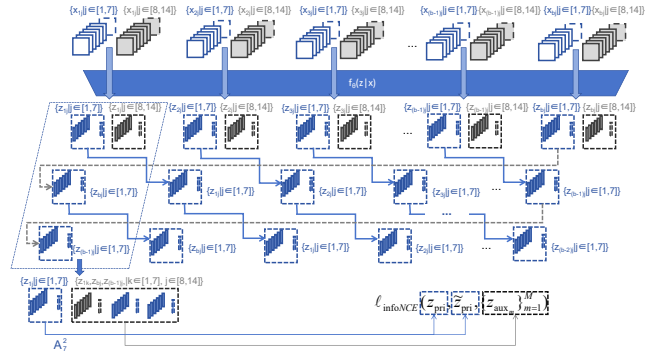


Fig. 6. Feedforward process of D2C phase 1

It is worth emphasizing that the improvement in model performance observed through the aforementioned approach is not solely attributed to an increase in the number of negative examples within each contrastive group. This paper posits that the incorporation of negative examples, which assist in delineating concept boundaries, holds the key to enhancing a model’s proficiency in abstract reasoning tasks. Merely augmenting the dataset with insignificant negative examples does not lead to substantial gains in model performance. In an attempt to enrich the dataset, this study generated a substantial amount of Bongard-logo virtual data using DDPM and integrated these as auxiliary data points within the original problems. However, subsequent analysis revealed that this methodology did not tangibly enhance model accuracy.

#### B. D2C phase 2: The concept delineation method based on a new loss function term

This paper posits that, in addition to altering the manner of sampling training data, establishing an extra loss function to constrain the similarity between the representations of the primary group samples across different cases within a batch of Bongard-Logo training data can implicitly achieve the fundamental objective of this paper.

Specifically, in this paper, we exclusively retain the primary representational components of all questions within the set

$\{Z_{ij} | i \in [1, b], j \in [1, 14]\}$ , which specifically correspond to  $\{Z_{ij} | i \in [1, b], j \in [1, 7]\}$ . Subsequently, we randomly partition the primary representation of each case within  $\{Z_{ij} | i \in [1, b], j \in [1, 7]\}$  into two distinct subsets:  $\{Z_{ih} | i \in [1, b]\}$  and  $\{Z_{i\bar{h}} | i \in [1, b]\}$ , where  $\{Z_{ih} | i \in [1, b]\} \cup \{Z_{i\bar{h}} | i \in [1, b]\} = \{Z_{ij} | i \in [1, b], j \in [1, 7]\}$  and  $\{Z_{ih}\} \cap \{Z_{i\bar{h}}\} = \emptyset$ . By aggregating the vectors within  $\{Z_{ih} | i \in [1, b]\}$  and  $\{Z_{i\bar{h}} | i \in [1, b]\}$ , we derive the corresponding vectors  $\{v_i | i \in [1, b]\}$  and  $\{\tilde{v}_i | i \in [1, b]\}$ . Ultimately, we compute InfoNCE loss function for constraining the similarity among  $\{v_i | i \in [1, b]\}$  and  $\{\tilde{v}_i | i \in [1, b]\}$  as the additional loss function item. The specific calculation process can be explained by:

$$\begin{aligned}
 \ell_{D2C}(\{z_{ij} | i \in [1, b], j \in [1, 7]\}) \\
 &= - \sum_{i=1}^b \log \frac{e^{(v_i \cdot \tilde{v}_i)/t}}{e^{(v_i \cdot \tilde{v}_i)/t} + \sum_{i=1, \tilde{i} \neq i}^b e^{(v_i \cdot \tilde{v}_{\tilde{i}})/t}} \\
 &\text{where } v_i = \sum \{Z_{ih}\}, \tilde{v}_i = \sum \{Z_{i\bar{h}}\} \\
 &\text{and } \{Z_{ih}\} \cup \{Z_{i\bar{h}}\} = \{Z_{ij} | j \in [1, 7]\}
 \end{aligned} \quad (6)$$

This loss term is to decrease the similarity of primary group representations across different cases. The schematic representation of the feedforward procedure is provided in the figure 7. Furthermore, the spirit of D2C method can be integrated with

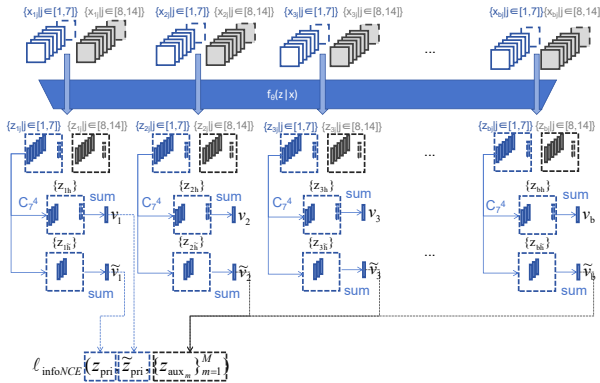


Fig. 7. Feedforward process of D2C phase 2

Lico-Net by introducing images from other case statements as negative examples within the cases. And this process is illustrated in figure 8.

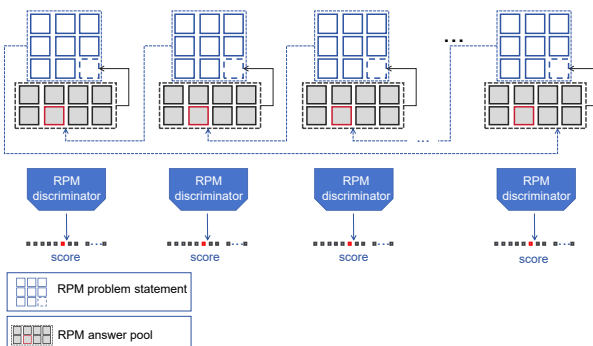


Fig. 8. Feedforward process of Lico-Net aligned with D2C

In summary, D2C is a unpretentious and effective approach. Since the determination of image attributes in Bongard-Logo relies heavily on the concepts delineated by the main and auxiliary groups within each case, D2C tackles the problem by decoupling the concepts between different cases. However, regarding the RPM problem, which remains consistency in the identification of image attributes, this paper holds a pessimistic view on the effectiveness of D2C in solving RPM.

## VI. DISTRIBUTION DISTANCE-BASED DISCRIMINATOR OF CASE (D3C)

Using distributions to describe human concepts in abstract reasoning problems for the deep networks is preferable to using vectors. Distributions offer a more comprehensive and nuanced approach to capturing the diversity and uncertainty inherent in human concepts. Human concepts are often ambiguous, polysemous, and subject to varying degrees and fluctuations, which can be challenging to represent using static vectors. In contrast, distributions provide a dynamic and probabilistic framework that can accommodate this inherent variability.

By leveraging distributions to represent human concepts, we can furnish deep networks with richer and more flexible information. This enhanced representational capacity enables the networks to better understand and address the complexity and uncertainty encountered in abstract reasoning problems. For instance, probability distributions can be utilized to depict the range of possibilities and variations associated with a concept, while Gaussian distributions can model the continuity, smoothness and even discreteness of a concept's underlying structure.

### A. D3C for Bongard-Logo

The ideal approach to address the Bongard-Logo problem involves training an encoder capable of encoding images from a Bongard-Logo case into representations, denoted as  $z$ . In this context, the representations of positive instances (samples in primary group) belong to the distribution  $p(z)$ , while the representations of negative instances (samples in primary group) belong to  $q(z)$ . Importantly, there should be minimal overlap between  $p(z)$  and  $q(z)$  in terms of cross-measure.

Specifically, this paper hypothesizes that the representation of the primary group samples in a Bongard-Logo case follows a Gaussian distribution, while the representation of the auxiliary group samples follows a mixed Gaussian distributions. We utilize an arbitrary backbone network  $g(z|x)$  to approximate the distribution of image representations within Bongard-Logo cases by converting the process of  $g(z|x)$  into  $g(\mu, \sigma|x)$ . The vector encoded by the backbone  $g(z|x)$  is divided into two equal-length segments. The first half of the encoded vector is treated as the mean of a Gaussian distribution, while the second half represents the logarithm of variance, effectively normalizing the output vectors into Gaussian distributions and distributing the image representations of Bongard-Logo case. Our approach mimics the form of Variational Autoencoder



(VAE). We posit that describing the image of case using distributions, rather than vectors, offers greater reasonableness.

With the estimated distributions of representations for each image in the Bongard-Logo cases, we compute the Sinkhorn distance between these distributions using reparameterization technique. Following the logical structure of each Bongard-Logo case, we impose constraints on these distances for the backbone network  $g(\mu, \sigma | x)$ , aiming to train an effective discriminator. Specifically, we optimize the network by utilizing a binary cross-entropy loss function to enforce constraints on the exponential function of the negative Sinkhorn distance with base  $e$  ( $e^D \in [0, 1]$ , where  $D \in [0, +\infty]$  is the values of Sinkhorn distance), aligning with the case's underlying logic mentioned in DC. This process can be expressed as figure 9. The D3C Method, applied to a batch of Bongard-Logo case distributions encoded by the backbone network  $g(\mu, \sigma | x)$ , can be expressed as follows:

$$\begin{aligned} \mathcal{L}_{D3C}(\{z_{ijs} | i \in [1, b], j \in [1, 14], s \in [1, S]\}) \\ = \sum_{i=1}^b \sum_{j=1}^7 \sum_{\tilde{j}=j+1}^7 \text{Sinkhorn}(z_{ijs}, z_{i\tilde{j}s}) \\ + \sum_{i=1}^b \sum_{j=1, \tilde{j}=7}^7 \log(1 - e^{-\text{Sinkhorn}(z_{ijs}, z_{i\tilde{j}s})}) \end{aligned} \quad (7)$$

$b$  is the batchsize of training.  $S$  is set to 20, and  $S$  represents the sampling frequency of the reparameterization technique.

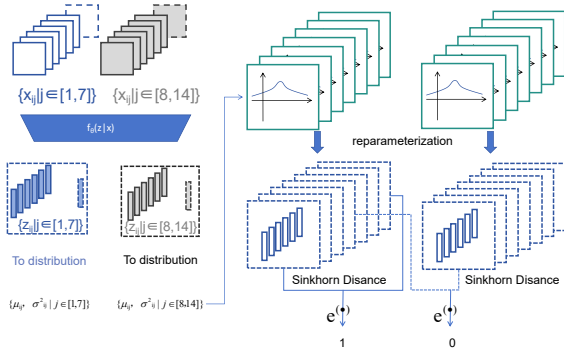


Fig. 9. Feedforward process of D3C

### B. D3C on Lico-Net for RPM

Notably, in contrast to the Bongard-Logo database, both RAVEN and PGM possess well-defined and comprehensive Meta data in the form of (auxiliary) rule labels. These rule descriptions facilitate the construction of a rational concept space, with non-overlapping concepts within the rule labels. This paper introduces the rule labels from the RPM database into the Lico-Net, aiming to enhance the reasoning accuracy and human-perspective rule interpretability of Lico-Net.

Specifically, under the rule description frameworks of RAVEN and PGM, there exists a many-to-one relationship between image progression patterns and rule. For instance, both single-step and double-step increments, as well as single-step and double-step decays in image attributes, are described as

rule: “progressive”. Therefore, this paper decides to distribute the concept of rule from the RPM database and vectorize the image progression patterns. We can leverage this approach to naturally constrain the image progression patterns within their corresponding rule distributions, thereby optimizing the deep model’s learning of rules and clarifying the boundaries among various concepts within the data.

In practice, we utilized a standard Transformer-Encoder to convert the textual descriptions of Meta data into concept vectors  $\{r_k | k \in [1, K]\}$ , where  $K$  represents the count of distinct rule description in Meta data. Specifically, the initial portion of the feature vector is designated as the mean  $\{\mu_k | k \in [1, K]\}$ , whereas the latter half signifies the logarithm of variance  $\{\log(\sigma_k^2) | k \in [1, K]\}$ , effectively distributing the rule descriptions and yielding a set of distributions  $\{\mu_k, \sigma_k^2 | k \in [1, K]\}$ . Lico-Net has inherently achieved the vectorization of image progression patterns, yielding vectors termed as progression pattern vectors. Consequently, we integrated a constraint term into Lico-Net, dictating that vectors representing progression patterns should exhibit a high likelihood of adhering to the distribution outlined by their corresponding textual rules, and conversely, demonstrate a low probability of deviation.

A specific RPM case is encoded into  $N \times M$  progression pattern vectors  $\{P_{nm} | n \in [1, N], m \in [1, M]\}$  from  $L$  viewpoints by Lico-Net as aforementioned. To align Lico-Net with the D3C framework, the number of encoding patterns  $N$  in Lico-Net is set according to the instance of the RPM problem, depending on the number of mutually decoupled concepts present in the Meta data of that instance. For example, in PGM, there are two such concepts: shape pattern and line pattern, and  $N$  is set to 2. The special setting of  $N$  in Lico-Net can be viewed as  $N$  slots, which can be aligned with the  $N$  decoupled concepts described in the Meta data, respectively. By synthesizing all perspectives—specifically, by calculating the mean of the progression pattern vectors  $\{P_{nm} | n \in [1, N], m \in [1, M]\}$  across all  $L$  viewpoints—Lico-Net encodes  $N \times M$  vectors, denoted as  $\{\bar{P}_{nm} | n \in [1, N], m \in [1, M]\}$ , representing the full-viewpoint progression patterns. This process can be expressed as:

$$\begin{aligned} \{\bar{P}_{nm} | n \in [1, N], m \in [1, M]\} \\ = \frac{1}{L} \sum_{l=1}^L \{P_{nm} | n \in [1, N], m \in [1, M]\}_l \end{aligned} \quad (8)$$

The  $l$  represents the index of viewpoints. The  $\{\bar{P}_{nm} | n \in [1, N], m \in [1, M]\}$  can be treated as  $N$  sets of  $M$  sampling results. This enables the optimization of distribution distances based on the Sinkhorn distance, thereby enhancing the overall performance. Apparently, this paper utilizes the Sinkhorn distance to constrain the distance between  $M$  progression pattern vectors and their corresponding distributions’ sampling results. The  $N$  decoupling concept presented in Meta data is employed to concurrently impose constraints on the  $N$  sets of  $M$  progression pattern vectors, and the calculate process can be expressed as:

$$\begin{aligned}
 & \ell_{D3C}(\{\bar{P}_{nm} | n \in [1, N], m \in [1, M]\}, \{r_{ks} | k \in [1, K], s \in [1, S]\}) \\
 &= \sum_{n=1, \tilde{k} | n}^N \text{Sinkhorn}(\bar{P}_{nm}, r_{\tilde{k}s}) \\
 &+ \sum_{k=1, k \neq \tilde{k}}^K \sum_{n=1, \tilde{k} | n}^N \log(1 - e^{-\text{Sinkhorn}(\bar{P}_{nm}, r_{ks})})
 \end{aligned} \quad (9)$$

The  $\bar{P}_{nm}$  represents the full-viewpoint progressive pattern vectors encoded by Lico-Net, and  $\{r_{ks}\}$  represents the  $S$  sampling results from the distribution  $\{\mu_k, \sigma^2_k\}$  of the rule description. It is evident that the specific value of  $\tilde{k}$  is contingent upon the description of Meta data corresponding to the particular case of the RPM problem. symbol “ $\tilde{k} | n$ ” represents that the specific value of  $\tilde{k}$  is depended on  $n$ . This dependency realizes the fact that each slots in Lico-Net are aligned with their corresponding concepts. The  $\text{Sinkhorn}(\cdot, \cdot)$  represents the Sinkhorn distance operator. The other logic of symbol in function (9) has mentioned. It becomes evident that we are employing the Binary Cross Entropy (BCE) loss function to impose constraints on the exponential negative Sinkhorn distance result. A more detailed feedforward process is illustrated in the figure 10.

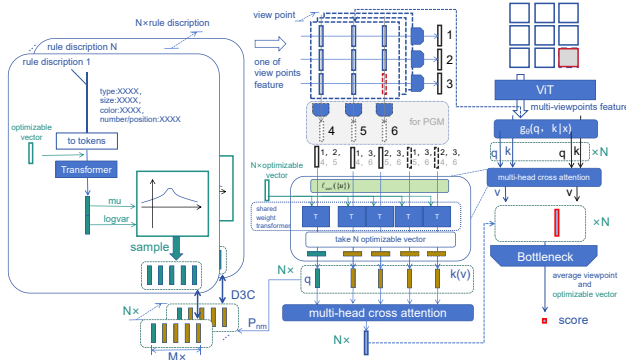


Fig. 10. Feedforward process of Lico-Net aligned with D3C

### C. A low-cost loss function for the D3C, the Hermes for the Zeus

Sampling  $S$  times (where  $S$  is arbitrarily set, and  $S$  is set to 20 for Sinkhorn distance) from the constructed distribution  $\{\mu_k, \sigma^2_k\}$  of concepts in Meta data and yielding  $\{r_{ks} | k \in [1, K], s \in [1, S]\}$ , we calculate the Sinkhorn distance between the progression pattern vectors and these sampling results  $\{r_{ks}\}$ . This Sinkhorn distance approximates the Wasserstein distance, which is currently a linear programming algorithm also known as the Earth Mover’s Distance (EMD) algorithm. Typically, this approach requires a substantial number of samples and incurs a considerable computational cost. Even if we treat the  $M$  progression pattern vectors as  $M$  sampling results, it is still difficult to satisfy the prerequisite of extensive sampling in the context of the RPM problem, where  $M$  is set to 9 in PGM and 3 in RAVEN. To reduce computational cost and sampling frequency, this paper employs cosine similarity between vectors as an alternative distance metric norm to the

Sinkhorn distance. Obviously, the cosine similarity satisfies with the *Lipschitz* continuity condition. For the inner product, treating it as a function with one fixed vector, we observe that it exhibits *Lipschitz* continuity. Specifically, given a fixed vector  $v$ , the function  $f(u) = u \cdot v$  is *Lipschitz* continuous with respect to  $u$ , with the *Lipschitz* constant  $L$  being equivalent to the norm of  $v$ . This property is attributed to the inner product’s adherence to the Cauchy-Schwarz inequality:  $|u \cdot v| \leq \|u\| \cdot \|v\|$ . Leveraging this inequality, we are able to deduce the underlying inequality:

$$f(u_1) - f(u_2) = |u_1 \cdot v - u_2 \cdot v| = |(u_1 - u_2) \cdot v| \leq \|u_1 - u_2\| \cdot \|v\| \quad (10)$$

In our study, we opted for cosine similarity, considering normalized vectors  $u$  and  $v$ , where  $\|v\|$  and  $\|u\|$  are equal to 1, and Lipschitz constant  $L = \|v\| = 1$ . It is reasonable to choose the mean of cosine similarity between sampling vectors as the distance metric function instead of Sinkhorn distance.

Correspondingly, due to the change in distance metric function, the range of function values also undergoes transformation. To be specific, the cosine similarity ranges from -1 to 1, whereas the Sinkhorn distance spans from 0 to positive infinity. Consequently, the range of values for the exponential function of the negative Sinkhorn distance with base  $e$  becomes 0 to 1. This alteration in value ranges led us to replace BCE with infoNCE as the loss function. The constraint logic of infoNCE is identical to the previously mentioned DC method. The calculate process of new method applied on Bongard-Logo can be expressed as:

$$\begin{aligned}
 & \ell_{D3C-\text{cos}}(\{z_{ijs} | i \in [1, b], j \in [1, 14], s \in [1, S]\}) \\
 &= - \sum_{i=1}^b \sum_{j=1}^7 \sum_{\tilde{j}=j+1}^7 \sum_{s=1}^S \log \frac{e^{(z_{ijs} \cdot z_{i\tilde{j}s})/t}}{e^{(z_{ijs} \cdot z_{i\tilde{j}s})/t} + \sum_{k=8}^{14} e^{(z_{ijs} \cdot z_{iks})/t}}
 \end{aligned} \quad (11)$$

The calculate process of new method aligned with Lico-Net can be expressed as:

$$\begin{aligned}
 & \ell_{D3C-\text{cos}}(\{\bar{P}_{nm} | n \in [1, N], m \in [1, M]\}, \{r_{ks} | k \in [1, K], s \in [1, S]\}) \\
 &= - \sum_{n=1, \tilde{k} | n}^N \sum_{m=1}^M \sum_{s=1}^S \log \frac{e^{(\bar{P}_{nm} \cdot r_{\tilde{k}s})/t}}{e^{(\bar{P}_{nm} \cdot r_{\tilde{k}s})/t} + \sum_{k=1, k \neq \tilde{k}}^K e^{(\bar{P}_{nm} \cdot r_{ks})/t}}
 \end{aligned} \quad (12)$$

The  $t$  is set to  $10^{-6}$  and  $S$  is set to 5 in function (11) and (12). The logic of symbols in function (11) and (12) has mentioned. It is evident that, compared to function (7) and (9), the demand for sampling frequency  $S$  in D3C-cos has been significantly reduced.

From a certain perspective, estimating the distribution distance based on cosine similarity between sampling results can be regarded as a variant of the Wasserstein distance based on cosine similarity that relinquishes the lower bound estimation and possesses a relatively low, fixed Lipschitz constant. Therefore, this method, we called “D3C-cos”, cannot precisely quantify the distance between distributions. It serves as a low-cost loss function for constrained inter-distribution distance, serving as a surrogate for the Sinkhorn distance, the Hermes for the Zeus.

The success of such simplification can be attributed, in part, to our modeling of the distribution of pattern descriptions as a Gaussian distribution. It is worth noting that the D2C and D3C methods are not in conflict. The D2C method attempts to redefine concept boundaries for reasoning problems. According to D3C, depicting concepts in the form of distributions is more reasonable compared to using vectors.

## VII. DEFENSE-DRIVEN DISCRIMINATION OF DISTRIBUTED CONCEPTS (D4C)

This paper aims to delineate more appropriate concept boundaries for the RPM and Bongard-Logo problems.

### A. Negative examples are not merely intended to confound the discriminator

This paper posits that it is worthwhile to consider the significance of positive and negative examples in abstract reasoning problems. Suppose that the correct solutions to each case in a reasoning problem follow a Gaussian distribution. Given that some reasoning problems may have multiple correct solutions, it is also possible that the distribution is a mixed Gaussian distribution. This is exemplified in datasets such as OIG and D9 from Raven database. One of the core challenges in RPM problems lies in the existence of multiple correct answers. While CRAB has eliminated this core difficulty through data cleaning in the RAVEN dataset, it has achieved noteworthy results on the cleaned version.

Currently, existing discriminative models for solving RPM and Bongard-Logo problems often adhere to a pattern where positive examples yield high probabilities when substituted into the case’s problem statement, while negative examples yield low probabilities. We can view this pattern in the following way: the discriminator constructs a solution distribution for the cases presented in abstract reasoning problems. Within this distribution, positive examples are assigned higher probabilities, whereas negative examples are assigned lower ones. The endeavor to train the discriminator can be conceptualized as a process of optimizing and fine-tuning the solution distribution, with the ultimate objective of aligning it more closely with the underlying distribution of correct solutions for the given cases. Using positive and negative examples to estimate a Gaussian distribution through the cross-entropy loss function can be seen as leveraging them to optimize the following function:

$$-\log(p(x, \mu, \sigma)) = \frac{(x_i - \mu_i)^2}{2\sigma_i^2} - \log(|\sigma_i|) - \frac{1}{2} \log(2\pi) \quad (13)$$

Where  $x$  represents the positive or negative samples,  $\mu$  and  $\sigma$  represent the mean and standard deviation of the Gaussian distribution separately. It can be observed that when positive instances are substituted into the formula, we aim for the smallest possible result, which corresponds to minimizing the mean squared loss between sample  $x$  and the mean of the correct solution  $\mu$ . Conversely, when negative instances are substituted, we desire the largest possible result, equivalent to minimizing the standard deviation  $\sigma$  of the respective segment.

Therefore, this paper posits that in reasoning problems, the establishment of positive examples aids deep models in estimating the mean of the correct solution distribution, while negative examples serve to estimate the variance. The variance represents the distance between the boundaries of the distribution and its center. Correspondingly, we posit that negative examples play a crucial role in abstract reasoning tasks, serving to delimit the concepts presented in each case. This underscores the significance of establishing both positive and negative examples in abstract reasoning problems. This significance reflects a despairing fact that the upper limit of the discriminator’s reasoning accuracy in this abstract reasoning problem is determined by the quality of positive and negative examples in the question.

### B. High-quality negative examples lead to more rigorous concept boundaries

Our proposed D2C method has outlined a new problem boundary for deep networks through the resampling of negative examples and the introduction of a new loss function. The experimental results merely suggest that this boundary is more suitable for the scenario of missing conceptual supervision signals compared to the boundary described by the original negative examples in Bongard-Logo. However, it remains uncertain whether the new boundary is too tight or not tight enough. In other words, D2C introduces a new variance in the solution distribution for the network, and whether this variance is larger or smaller compared to the variance of the correct solution distribution is uncertain. In the context of the Bongard-Logo problem, when there is no concept supervision signal, the variance provided by D2C is closer to the variance of the correct solution distribution compared to the variance described by the original negative examples.

Clearly, D2C has specific requirements for the dataset. As expected, empirical findings indicate that this method is insufficient for defining more precise boundaries in the context of the RPM problem. Contrary to Bongard-Logo problems, the RPM problems claim that different cases share a core set of concepts, ensuring discreteness and stability among them. This shared nature renders methods like D2C unsuitable for addressing RPM problems. In other words, image attributes within RPM cases are strictly constrained by definitions of “rules” or “progressive patterns”, maintaining consistency in ascribed values across all RPM cases. The varying attributions of image properties in the Bongard-Logo problem resulting from different clustering basis among cases, which adds to problem complexity and difficulty, the inclusion of positive examples from other cases as negative examples can delineate concept boundaries between two distinct cases to some extent, adhering to a cautious approach to minimize concept infringement. However, this strategy is clearly inapplicable when dealing with RAVEN and PGM problems due to significant differences in multiple aspects.

This paper introduces a novel approach that aims to provide a tighter boundary for the discriminator by continuously generating confusing representations and challenging the discriminator. Through iterative rounds of defending against the attacks

from generator, the discriminator enhances its discrimination and classification abilities, resulting in improved performance and accuracy.

C. discriminator for Bongard-logo

Effective Bongard-Logo discriminators are abundant, with our preceding works such as PMoC and Triple-CFN demonstrating notable success. These discriminators are amenable to integration with the D2C and D3C methods proposed in this paper, and we have conducted pertinent experiments to explore their combination. These discriminators have exhibited their proficiency in accurately identifying and classifying Bongard-Logo cases, contributing significantly to the advancement of research in this domain.

With regards to discriminators capable of handling adversarial tasks, the Wasserstein GAN, an excellent adversarial generative network, proposes a noteworthy requirement. The discriminator must be able to undertake a task that involves measuring the distance between samples generated by the generator and real samples. This necessitates that the discriminator must satisfy Lipschitz continuity to a certain extent.

In this paper, the choice of PMoC constrained by spectral normalization as the discriminator for the D4C method on Bongard-logo is motivated by the explicit measurement of the distance between auxiliary group sample and primary group sample distributions provided by the PMoC approach. In contrast, the task of Triple-CFN is relatively more complex, as it not only measures the distance between primary and auxiliary samples but also considers the distance between primary samples. Therefore, compared to PMoC, this article has more design for the generator of Triple-CFN.

D. generator for Bongard-logo

This paper argues that, instead of forcing the generator to produce samples that can confuse the discriminator, it is more effective to generate representations of samples. In terms of the intuitive metric of computational complexity, this approach reduces the pressure on the network.

For the Bongard-Logo problem, this paper models the overall distribution as a mixed Gaussian distribution. Within this framework, each individual primary group in a Bongard-Logo case is modeled as a separate Gaussian distribution. Consequently, the generator of D4C designed for the Bongard-Logo problem possesses a relatively straightforward structure. The generator’s objective is to encode a distribution based on the representations of the primary group in a given Bongard-Logo case, ensuring that any representation sampled from this distribution is capable of effectively confusing the discriminator.

Specifically, we use a standard Transformer-Encoder to encode a Gaussian distribution based on the primary samples’ representations in a Bongard-Logo cases, along with one optimizable vectors. The encoding approach is similar to D3C, where we extract the optimizable vector from the attention results and process it through a linear feed-forward layer to obtain the mean and variance logarithm of a Gaussian distribution. We then sample multiple representations from

this distribution as confusing representations to challenge the discriminator, which must exert maximum effort to counter them. The training objective of the generator is to generate representations for Bongard-Logo cases that achieve higher scores in the discriminator compared to the representations of the original negative examples in the case. However, the training objective of the discriminator is clear-cut: to classify these generated representations as negative examples. The alignment of the generator and PMoC is illustrate in figure 11. The “ $f_{\theta}(z_{ij}|x_{ij})$ ” and “ $g_{\omega}(p'_i(z_{ij}|y)|\{z_{ij}\}_{j=1}^6, z_{ij}')$ ” in figure

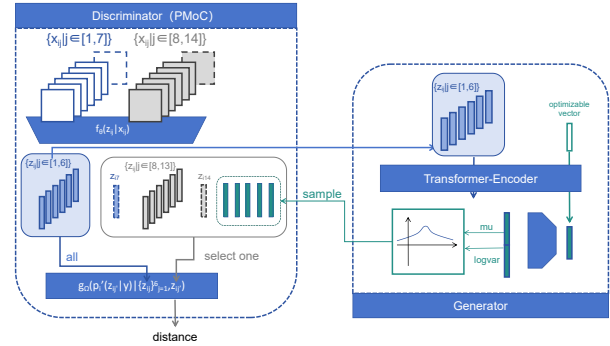


Fig. 11. Feedforward process of D4C aligned with PMoC on Bongard-Logo

11 is the perceptron and logic calculation module in PMoC.

For the generator of Triple-CFN, it is necessary to decay the generated representations. Specifically, when the generator with aforementioned structure produces a confusing representation for Triple-CFN, this confusing representation needs to be weighted and summed with the representations in the auxiliary group. After taking the average of the representations in the auxiliary group, it is weighted and summed with the confusing representation in a ratio of 0.9:0.1 to decay the confusing representation vector. This is due to the mechanism of Triple-CFN, which defines the identity of an image based on the direction of its representation, making it easy for a generator based on the Transformer-Encoder to generate realistic confusing representations, causing Triple-CFN to collapse. Therefore, this article designs the above decay process. The alignment of the generator and Triple-CFN is illustrate in figure 12. The “ $f_{\theta}(z_{ij}|x_{ij})$ ” in figure 12 is the encoder in Triple-CFN.

Finally, in the realm of abstract reasoning problems, particularly those involving generating answer samples, this paper believes that the D4C approach can also make valuable contributions. This opens up new avenues of exploration for future work, presenting challenges that are yet to be tackled.

E. discriminator of RPM

In terms of discriminating RPM problems, this paper places significant faith in the Lico-Net model as an exceptional baseline. The spectral normalization is anticipated to elevate Lico-Net’s performance, making it a highly suitable discriminator for the D4C method.

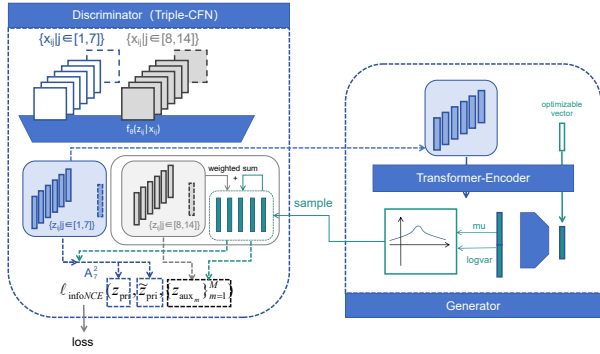


Fig. 12. Feedforward process of D4C aligned with Triple-CFN on Bongard-Logo

F. generator of RPM

Distinct from the Bongard-Logo problem, the answer for a single case in the RPM problem can be represented as a mixed Gaussian distributions due to its non-uniqueness. Thus, Our aspiration is for the generator, tailored for the D4C method within the RPM context, to encode a distribution that represents a mixed Gaussian distribution. This paper employs a glove-shaped network to simulate the process of sampling from a mixed Gaussian distributions. Specifically, we utilize a standard Transformer-Encoder to process the representations of all the problem images in an RPM case, along with  $W$  optimizable vectors (where  $W$  is a hyperparameter.) and a stochastic promoter (these  $W + 1$  vectors, when arranged together, surprisingly resemble the shape of a glove). The promoter is a vector sampled from a multivariate Gaussian distribution, where the mean of the distribution is optimizable while the variance is fixed at 1.

It is worth noting that we have designed a novel positional encoding embedding method for the backbone of our RPM generator, the Transformer-Encoder, to restore the  $3 \times 3$  image arrangement of the RPM problem matrix. For the PGM problem, our positional encoding scheme involves assigning unique encodings to images located on the diagonal and upper triangular regions within the problem matrix of a given PGM case. The positional encodings for images in the lower triangular region are correspondingly symmetrical with respect to the diagonal, mirroring the encodings of their counterparts in the upper triangular region. However, this paper does not demonstrate the superiority of D4C on the relatively less challenging RAVEN dataset.

Back to the main topic. After obtaining the attention results from the Transformer-Encoder, we extract  $W$  optimizable vectors from the attention results and process them into  $W$  distributions using a linear layer like aforementioned. Following the extraction of the promoter, it is processed into a probability output using a linear layer and hard-gumbel-softmax, yielding highlighted probabilities for the  $W$  distributions. We then sample representations as confusing representations from the highlighted distributions each time. In the technical implementation, we employed the reparameterization trick to draw samples from each distribution, yielding  $W$  sampling results. Subsequently, we performed a weighted sum of these sampling

results using the hard probabilities outputted by the hard-gumbel-softmax, thus completing the entire mixed-Gaussian sampling process. The approach for modeling and training the network, as presented in this paper, is coined as ‘‘D4C glove-train’’. A more elaborate illustration of the forward process is provided in the accompanying figure 13.

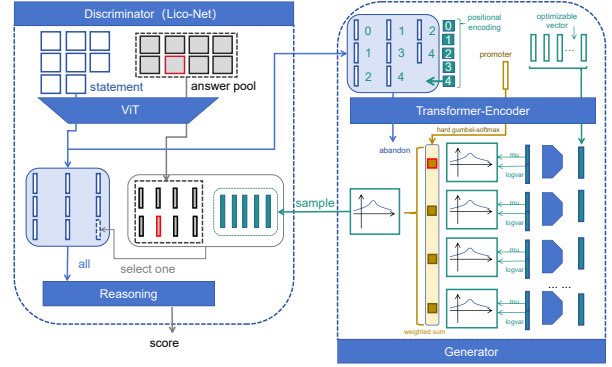


Fig. 13. Feedforward process of D4C on RPM problem

VIII. EXPERIMENT

All experiments conducted in this paper were programmed in Python, utilizing the PyTorch [43] framework.

A. Experiment on RAVEN

Initially, we conducted experiments with Lico-Net on both RAVEN [15] and I-RAVEN [37] datasets to demonstrate its inherent superiority. To ensure a fair comparison between excellent models, all experimental settings and equipment in this study were kept consistent with those of RS-Tran and Triple-CFN, including data volume, optimizer parameters, data augmentation methods (such as reducing the RAVEN image size to  $80 \times 80$ ), batch size, and other relevant hyperparameters.

TABLE II  
REASONING ACCURACIES ON RAVEN AND I-RAVEN.

Model	Test Accuracy(%)							
	Average	Center	2 × 2 Grid	3 × 3 Grid	L-R	U-D	O-IC	O-IG
SAVIR-T [24]	94.0/98.1	97.8/99.5	94.7/98.1	83.8/93.8	97.8/99.6	98.2/99.1	97.6/99.5	88.0/97.2
SCL [23], [24]	91.6/95.0	98.1/99.0	91.0/96.2	82.5/89.5	96.8/97.9	96.5/97.1	96.0/97.6	80.1/87.7
MRNet [21]	96.6/-	-/-	-/-	-/-	-/-	-/-	-/-	-/-
RS-TRAN [28]	98.4/98.7	99.8/100.0	99.7/99.3	95.4/96.7	99.2/100.0	99.4/99.7	99.9/99.9	95.4/95.4
Triple-CFN [32]	99.6/99.8	100.0/100.0	99.7/99.8	98.8/99.4	99.9/100.0	99.9/100.0	99.9/99.9	99.2/99.2
Lico-Net	99.7/99.8	100.0/100.0	99.7/99.8	98.9/99.5	99.9/100.0	99.9/100.0	99.9/99.9	99.4/99.6

B. Experiment on Bongard-Logo

Consequently, we conducted experiments on Bongard-Logo using ResNet50 and Triple-CFN as backbones for D2C, D3C, and D4C. The experimental results are presented in the table III. In the experiment with D3C, we conducted an additional experiment on its lightweight version, D3C-cos, to verify that replacing D3C with D3C-cos would not significantly affect performance. As can be seen in the table III, we did not conduct an experiment with Triple-CFN+D3C due to the large model size of Triple-CFN. This made it impractical to deploy

the model using conceptual distribution and logical optimization with the Sinkhorn distance on our existing experimental equipment. This was the driving force behind proposing D3C-cos as an alternative to D3C in this paper. In addition, the combination of D4C and PMoC+Straw Pose-Transformer has not been implemented due to limitations in computing power.

TABLE III  
REASONING ACCURACIES OF MODELS ON BONGARD-LOGO.

Model	Accuracy(%)				
	Train	FF	BA	CM	NV
SNAIL	59.2	56.3	60.2	60.1	61.3
ProtoNet	73.3	64.6	72.4	62.4	65.4
MetaOptNet	75.9	60.3	71.6	65.9	67.5
ANIL	69.7	56.6	59.0	59.6	61.0
Meta-Baseline-SC	75.4	66.3	73.3	63.5	63.9
Meta-Baseline-MoCo [42]	81.2	65.9	72.2	63.9	64.7
WReN-Bongard	78.7	50.1	50.9	53.8	54.3
SBSD	83.7	75.2	91.5	71.0	74.1
PMoC	92.0	92.6	97.7	78.3	75.0
PMoC+Straw Pose-Transformer	96.2	96.0	98.5	78.5	75.3
Triple-CFN	93.2	92.0	99.2	80.8	79.1
ResNet50	92.0	88.9	98.1	76.1	76.0
ResNet50+D2C	92.4	90.7	99.0	77.0	77.5
ResNet50+D3C	91.2	91.0	98.5	75.5	76.9
ResNet50+D2C+D3C	96.6	93.2	99.6	78.8	78.8
ResNet50+D3C-cos	95.2	90.2	98.8	79.0	78.1
ResNet50+D2C+D3C-cos	<b>96.0</b>	<b>92.3</b>	98.8	<b>79.8</b>	<b>79.1</b>
Triple-CFN+D2C	96.5	94.8	99.4	79.5	81.6
Triple-CFN+D3C-cos	97.0	96.2	99.4	82.0	79.7
Triple-CFN+D2C+D3C-cos	97.2	<b>96.2</b>	99.4	82.8	82.7
Triple-CFN+D4C	<b>97.7</b>	93.5	<b>99.6</b>	<b>82.8</b>	<b>83.1</b>
PMoC+D2C	93.9	95.0	98.1	78.5	78.4
PMoC+Straw Pose-Transformer+D2C	<b>98.7</b>	<b>96.8</b>	98.9	81.3	75.6
PMoC+D4C	96.0	95.2	<b>99.2</b>	<b>84.8</b>	<b>82.8</b>

Upon observing the results presented in the table III, we found that D2C, D3C, and D3C-cos made considerable contributions in the Bongard-Logo task, with D3C-cos emerging as an effective alternative to D3C. Additionally, D4C achieved remarkable results, despite not obtaining the best performance across all test data, possibly due to the inherent limitations of the PMoC model. However, compared to its backbone, PMoC, D4C demonstrated significant improvement and contribution, validating the effectiveness of defining tighter problem boundaries for the model. This approach warrants further investigation and development in future research.

### C. Experiment on PGM

In this paper, we conducted experiments related to Lico-Net on PGM. And the results are recorded in Tabel IV. In the experimental results recorded in Tabel IV, we can observe various phenomena. Lico-Net, in essence, addresses the imperfections within the Triple-CFN framework. In Triple-CFN, concepts and minimal reasoning units serve as queries and

TABLE IV  
REASONING ACCURACIES OF MODELS ON PGM.

Model	Test Accuracy(%)
SAVIR-T [24]	91.2
SCL [23], [24]	88.9
MRNet [21]	94.5
RS-CNN [28]	82.8
RS-TRAN [28]	97.5
Triple-CFN [32]	97.8
Triple-CFN+Re-space layer [32]	98.2
Triple-CFN+Re-space layer+D2C	98.3(98.25)
Lico-Net	98.5(98.52)
Lico-Net+D2C	98.5(98.53)
D4C (with Lico-Net as the backbone)	98.6(98.64)
D4C glove-train(with Lico-Net as the backbone)	<b>98.7</b> (98.73)
Meta Triple-CFN+Re-space layer [32]	99.3
Triple-CFN+Re-space layer+D3C	<b>99.4</b> (99.36)
Triple-CFN+Re-space layer+D3C-cos	<b>99.4</b> (99.37)
Meta Lico-Net	99.3(99.30)
Lico-Net+D3C	<b>99.4</b> (99.35)
Lico-Net+D3C-cos	<b>99.4</b> (99.38)

key-value pairs, respectively, for computing cross-attention outcomes. However, a fundamental flaw in its design lies in the logical hierarchy mismatch between concepts and minimal reasoning units. Specifically, concepts often require the combined expression of multiple minimal reasoning units. Despite this shortcoming, Triple-CFN remains a remarkable model. Lico-Net, born from the rectification of these imperfections, has achieved a little improvements in accuracy.

The combination of Lico-Net and D2C, and the combination of Triple-CFN and D2C, did not bring significant improvement, with the enhancement only reflected in the percentile of reasoning accuracy. This phenomenon was anticipated in this paper, as we believe it is due to the difference between RPM and Bongard-Logo problems. In RPM problems, different cases share the same concept space and attribute recognition method. However, the combination of D4C and D4C glove-train significantly improved Lico-Net’s performance. Additionally, the glove-shaped generator proved to be more suitable for generating negative representations of RPM problems, challenging Lico-Net and enabling it to achieve further refinement.

The combination of Lico-Net and D3C is noteworthy. To demonstrate the effectiveness of D3C’s approach to describing abstract concepts through distributions, this paper conducted experiments using Meta Lico-Net. Unlike “Lico-Net+D3C”, which encodes the description of image progressive patterns into distributions using a Transformer-Encoder, Meta Lico-Net encodes them into vectors. To simplify, instead of dividing the encoded representation into mu and logvar, we directly utilize the representation as a vector. Furthermore, the cosine distance between progressive pattern vectors  $\{P_{nm}\}$  and the vectorized

pattern description in Lico-Net is constrained using infoNCE. In fact, the process mentioned above is an emulation of how Triple-CFN evolved into Meta Triple-CFN. The structure of Meta Lico-Net is illustrate in figure 14. The intention behind establishing Meta Lico-Net and Triple-CFN+D3C is to demonstrate that, compared to vectors, distributions are more suitable for describing abstract concepts. To further validate the theme of D3C, we applied both D3C and D3C-cos to Triple-CFN and Lico-Net. Through experimentation, we found that D3C and D3C-cos brought improvements to Triple-CFN, elevating its performance to the level of Lico-Net.

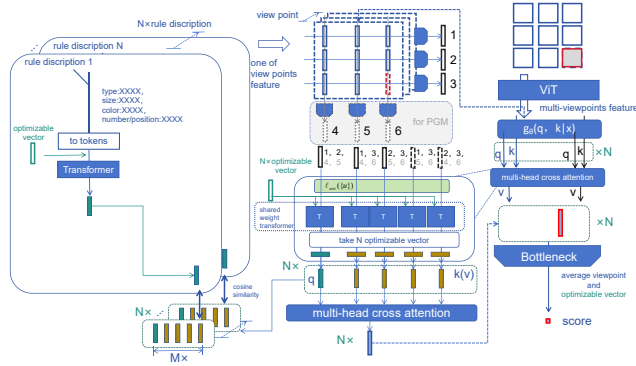


Fig. 14. Feedforward process of Meta Lico-Net

TABLE V  
PROGRESSIVE PATTERN REASONING ACCURACIES AND OF MODELS ON PGM.

Model	Accuracy(%)		
	shape	line	answer
Meta Triple-CFN [32]	99.5	99.9	98.4
Meta Triple-CFN+Re-space layer [32]	99.7	99.9	99.3
Meta Lico-Net	99.7	99.9	99.3
Lico-Net+D3C	99.7	99.9	99.4
Lico-Net+D3C-cos	99.7	99.9	99.4

The D3C’s reasoning accuracys of progressive pattern are recorded in Table V, highlighting the strong interpretability prior to training possessed by both D3C and Lico-Net. This exceeds that of Rs-Tran and its derivative, Tran-clip. It must be acknowledged that the experiment of applying D3C, which is based on the Sinkhorn distance, to Lico-Net was not conducted to its fullest extent in this paper. Once the experimental results of Lico-Net+D3C were sufficient to illustrate our point, we halted the model training. This was due to the significant computational resources required, even with the experimental equipment used in this paper: four A100s graphics cards. The training involved numerous epochs and tedious individual training epochs. This was the intended purpose behind the design of D3C-cos as a replacement for D3C, as the power of Zeus needs to be conveyed by Hermes.

#### D. Ablation experiment on D2C

In the final of this section, we devised an experiment to validate the D2C approach. Utilizing a 500-step DDPM model,

we generated a substantial quantity of Bongard-Logo data, specifically 3,180 Bongard-Logo images. According to the DDPM theory, these images belong to the same distribution as the real data, albeit with unknown semantics and concepts. During the training of ResNet50 and Triple-CFN, for each feedforward pass, we introduced 14 randomly selected DDPM-generated images as auxiliary group examples for the Bongard-Logo cases. The experimental results were recorded in “D2C-” item of the Table VI. It can be observed from the

TABLE VI  
REASONING ACCURACIES OF MODELS ON BONGARD-LOGO.

Model	Accuracy(%)				
	Train	FF	BA	CM	NV
ResNet50	92.0	88.9	98.1	76.1	76.0
Triple-CFN	93.2	92.0	99.2	80.8	79.1
ResNet50+D2C	92.4	90.7	99.0	77.0	77.5
Triple-CFN+D2C	96.5	94.8	99.4	79.5	81.6
ResNet50+D2C-	93.5	84.2	99.5	77.0	76.2
Triple-CFN+D2C-	95.7	93.2	98.9	79.3	80.9

experiment results recorded in Table VI that introducing generated samples as negative examples is difficult to fundamentally alter the network’s performance, as such behavior struggles to reorganize the concepts. In other words, D2C is restructuring the conceptual space, and the new concept space is highly coupled with the image style, with mutual exclusion between different cases of concepts. When the images generated by DDPM are introduced as auxiliary images into the Bongard-Logo case, they cannot achieve the above goal. Because D2C does not stop at the surface, that is, adding more auxiliary images to the Bongard-Logo case.

## IX. CONCLUSION

In summary, D2C presents a novel approach to tackling Bongard-Logo and RPM problems by resampling training data and introducing new loss function terms, effectively outlining new boundaries for solutions to these challenges. However, the extent to which these boundaries adapt to the specific problems remains uncertain. Conversely, D3C advocates for representing concepts in abstract reasoning problems using distributions. It posits that, compared to vectors, distributions are better suited to capture the high-dimensionality, abstractness, and complexity inherent in human concepts, and experimental evidence underscores the superiority of this approach.

D4C builds upon the principles of both D2C and D3C, exploring the roles of positive and negative examples in abstract reasoning problems from a perspective on distribution. Specifically, positive examples are utilized to depict the mean for deep networks, while negative examples contribute to describing the variance. Based on this understanding, D4C employs an adversarial approach, pitting the generator against the discriminator in repeated challenges. The generator continually produces negative examples that push the boundaries of

the problem, while the discriminator refines its skills through repeated defense.

This iterative process not only enhances the discriminator’s ability to distinguish between genuine and generated examples but also improves the generator’s capacity to generate more sophisticated negative examples. Ultimately, this adversarial framework promotes the evolution of both components, leading to more robust and reliable solutions in abstract reasoning tasks.

## REFERENCES

- [1] Deng, J., Dong, W., Socher, R., Li, L. J., Li, K., & Fei-Fei, L. Imagenet: A large-scale hierarchical image database. In *IEEE Conference on Computer Vision and Pattern Recognition*, 246-255 (2009).
- [2] Krizhevsky, A., Sutskever, I., & Hinton, G. E. Imagenet classification with deep convolutional neural networks. *Communications of the ACM*, 60(6), 84-90 (2017).
- [3] He, K., Zhang, X., Ren, S., & Sun, J. Deep Residual Learning for Image Recognition. In *IEEE Conference on Computer Vision and Pattern Recognition*, 770-778 (2016).
- [4] Vaswani, A. *et al.* Attention is All You Need. In *Advances in Neural Information Processing Systems*, (2017).
- [5] Devlin, J., Chang, M. W., Lee, K., & Toutanova, K. Bert: Pre-training of Deep Bidirectional Transformers for Language Understanding. Preprint at <https://arxiv.org/abs/1810.04805> (2018).
- [6] Brown, T. *et al.* Language Models are Few-shot Learners. In *Advances in Neural Information Processing Systems*, 1877-1901 (2020).
- [7] Goodfellow, I. *et al.* Generative adversarial networks. *Communications of the ACM*, 63(11), 139-144 (2020).
- [8] Kingma, D. P., & Welling, M. Auto-encoding variational bayes. Preprint at <https://arxiv.org/abs/1312.6114> (2014).
- [9] Ho, J., Jain, A., & Abbeel, P. Denoising diffusion probabilistic models. In *Advances in Neural Information Processing Systems*, 33, 6840-6851 (2020).
- [10] Antol, S., Agrawal, A., Lu, J., Mitchell, M., Batra, D., Zitnick, C. L., & Parikh, D. VQA: Visual question answering. In *IEEE International Conference on Computer Vision*, 2425-2433 (2015).
- [11] Johnson, J., Hariharan, B., Van Der Maaten, L., Fei-Fei, L., Lawrence Zitnick, C., & Girshick, R. Girshick. CLEVR: A Diagnostic Dataset for Compositional Language and Elementary Visual Reasoning. In *IEEE Conference on Computer Vision and Pattern Recognition*, 2901-2910 (2017).
- [12] Depeweg, S., Rothkopf, C. A., & Jäkel, F. Solving Bongard Problems with a Visual Language and Pragmatic Reasoning. Preprint at <https://arxiv.org/abs/1804.04452> (2018).
- [13] Nie, W., Yu, Z., Mao, L., Patel, A. B., Zhu, Y., & Anandkumar, A. Bongard-LOGO: A New Benchmark for Human-Level Concept Learning and Reasoning. In *Advances in Neural Information Processing Systems*, 16468-16480 (2020).
- [14] Raven J. C. Raven’s Progressive Matrices. (Western Psychological Services, (1938).
- [15] Zhang, C., Gao, F., Jia, B., Zhu, Y., & Zhu, S. C. Raven: A Dataset for Relational and Analogical Visual Reasoning. In *Proceedings of the IEEE/CVF Conference on Computer Vision and Pattern Recognition*, 5317-5327 (2019).
- [16] Barrett, D., Hill, F., Santoro, A., Morcos, A., & Lillicrap, T. Measuring Abstract Reasoning in Neural Networks. In *International Conference on Machine Learning*, 511-520 (2018).
- [17] Dosovitskiy, A. *et al.* An Image is Worth 16x16 Words: Transformers for Image Recognition at Scale. Preprint at <https://arxiv.org/abs/2010.11929> (2020).
- [18] Zheng, K., Zha, Z. J., & Wei, W. Abstract Reasoning with Distracting Features. In *Advances in Neural Information Processing Systems*, (2019).
- [19] Zhang, C., Jia, B., Gao, F., Zhu, Y., Lu, H., & Zhu, S. C. Learning Perceptual Inference by Contrasting. In *Proceedings of Advances in Neural Information Processing Systems*, (2019).
- [20] Zhuo, T., & Kankanhalli, M. Effective Abstract Reasoning with Dual-Contrast Network. In *Proceedings of International Conference on Learning Representations*, (2020).
- [21] Benny, Y., Pekar, N., & Wolf, L. Scale-Localized Abstract Reasoning. In *Proceedings of the IEEE/CVF Conference on Computer Vision and Pattern Recognition*, 12557-12565, (2021).
- [22] Zhuo, Tao and Huang, Qiang & Kankanhalli, Mohan. Unsupervised abstract reasoning for raven’s problem matrices. *IEEE Transactions on Image Processing*, 8332-8341, (2021).
- [23] Wu, Y., Dong, H., Grosse, R., & Ba, J. The Scattering Compositional Learner: Discovering Objects, Attributes, Relationships in Analogical Reasoning. Preprint at <https://arxiv.org/abs/2007.04212> (2020).
- [24] Sahu, P., Basioti, K., & Pavlovic, V. SAViR-T: Spatially Attentive Visual Reasoning with Transformers. Preprint at <https://arxiv.org/abs/2206.09265> (2022).
- [25] Zhang, C., Jia, B., Zhu, S. C., & Zhu, Y. Abstract Spatial-Temporal Reasoning via Probabilistic Abduction and Execution. In *Proceedings of the IEEE/CVF Conference on Computer Vision and Pattern Recognition*, 9736-9746 (2021).
- [26] Zhang, C., Xie, S., Jia, B., Wu, Y. N., Zhu, S. C., & Zhu, Y. Learning Algebraic Representation for Systematic Generalization. In *Proceedings of the European Conference on Computer Vision*, (2022).
- [27] Hersche, M., Zeqiri, M., Benini, L., Sebastian, A., & Rahimi, A. A Neuro-vector-symbolic Architecture for Solving Raven’s Progressive Matrices. Preprint at <https://arxiv.org/abs/2203.04571> (2022).
- [28] Q. Wei, D. Chen, B. Yuan, Multi-viewpoint and multi-evaluation with felicitous inductive bias boost machine abstract reasoning ability, *arXiv* :2210.14914, 2022.
- [29] Shi, Fan, Bin Li, and Xangyang Xue. "Abstracting Concept-Changing Rules for Solving Raven’s Progressive Matrix Problems." *arxiv preprint arXiv:2307.07734* (2023).
- [30] S.Kharagorgiev, "Solvingbongardproblemswithdeeplearning," k10v.github.io,2020.
- [31] R.Song, B.Yuan. Solving the bongard-logo problem by modeling a probabilistic model. Preprint at [https://arxiv.org/abs/ arXiv:2403.03173](https://arxiv.org/abs/arXiv:2403.03173) (2024).
- [32] R.Song, B.Yuan. Triple-CFN: Restructuring Conceptual Spaces for Enhancing Abstract Reasoning process. Preprint at <https://arxiv.org/abs/arXiv:2403.03190> (2024).
- [33] Shen, Jian, et al. "Wasserstein distance guided representation learning for domain adaptation." *Proceedings of the AAAI Conference on Artificial Intelligence*. Vol. 32. No. 1. 2018.
- [34] Cuturi, Marco. "Sinkhorn distances: Lightspeed computation of optimal transport." *Advances in neural information processing systems* 26 (2013).
- [35] Miyato, Takeru, et al. "Spectral normalization for generative adversarial networks." *arxiv preprint ar\*\*v:1802.05957* (2018).
- [36] Arjovsky, Martin, Soumith Chintala, and Léon Bottou. "Wasserstein generative adversarial networks." *International conference on machine learning*. PMLR, 2017.
- [37] Hu, S., Ma, Y., Liu, X., Wei, Y., & Bai, S. Stratified Rule-Aware Network for Abstract Visual Reasoning. In *Proceedings of the AAAI Conference on Artificial Intelligence*, 1567-1574 (2021).
- [38] Zhuo, T., Huang, Q., & Kankanhalli, M. Unsupervised Abstract Reasoning for Raven’s Problem Matrices. *IEEE Transactions on Image Processing*, 8332 - 8341 (2021).
- [39] Carpenter, P. A., Just, M. A., & Shell, P. What One Intelligence Test Measures: a Theoretical Account of the Processing in the Raven Progressive Matrices Test. *Psychological review*, 97(3), 404, (1990).
- [40] Chen, T., Kornblith, S., Norouzi, M., & Hinton, G. A Simple Framework for Contrastive Learning of Visual Representations. In *Proceedings of the International Conference on Machine Learning*, 1597-1607 (2020).
- [41] Oord, A. V. D., Li, Y., & Vinyals, O. Representation Learning with Contrastive Predictive Coding. Preprint at <https://arxiv.org/abs/1807.03748> (2019).
- [42] He, K., Fan, H., Wu, Y., Xie, S., & Girshick, R. Momentum Contrast for Unsupervised Visual Representation Learning. In *Proceedings of the IEEE/CVF Conference on Computer Vision and Pattern Recognition*, 9729-9738 (2020).
- [43] Paszke, A. *et al.* Automatic Differentiation in Pytorch. In *NIPS Autodiff Workshop*. (2017).